Modulation properties and nonlinear dynamics induced by optical feedback in distributed-feedback quantum cascade lasers

APL Photonics

RESEARCH ARTICLE | AUGUST 29 2025

# Modulation properties and nonlinear dynamics induced by optical feedback in distributed-feedback quantum cascade lasers

S. Zaminga ; L. Columbo ; C. Silvestri ; M. Gioannini ; F. Grillot



*APL Photonics* 10, 086114 (2025)
https://doi.org/10.1063/5.0252956

# Modulation properties and nonlinear dynamics induced by optical feedback in distributed-feedback quantum cascade lasers

Cite as: APL Photon. 10, 086114 (2025); doi: 10.1063/5.0252956
Submitted: 13 December 2024 • Accepted: 9 August 2025 •
Published Online: 29 August 2025



S. Zaminga,[1,a)] L. Columbo,[2] C. Silvestri,[3] M. Gioannini,[2] and F. Grillot[1,4]

## AFFILIATIONS

[1] LTCI Télécom Paris, Institut Polytechnique de Paris, Palaiseau 91120, France
[2] Dipartimento di Elettronica e Telecomunicazioni, Politecnico di Torino, Torino 10129, Italy
[3] Institute of Photonics and Optical Science (IPOS), School of Physics, The University of Sydney, Sydney NSW2006, Australia
[4] Centre d'Optique Photonique et Lasers, Université Laval, G1V 0A6 Quebec City, Canada

[a)] **Author to whom correspondence should be addressed:** sara.zaminga@telecom-paris.fr

## ABSTRACT

This study explores the dynamic behavior of distributed-feedback quantum cascade lasers (QCLs) through numerical simulations based on the Effective Semiconductor Maxwell–Bloch Equations (ESMBEs). First, we analyze the intrinsic intensity modulation response of QCLs, demonstrating that the modulation bandwidth is fundamentally constrained by the population grating induced by the standing-wave pattern in the QCL cavity, namely, spatial hole burning (SHB). We then extend the ESMBEs framework to incorporate the effects of an external target, enabling the investigation of multimode nonlinear dynamics in QCLs subject to external optical feedback (EOF). Our findings identify fast SHB and a non-zero linewidth enhancement factor as key physical mechanisms governing the emergence of complex multimode behavior and the eventual transition to chaos. Notably, we reveal that QCL destabilization under EOF arises from interactions between internal longitudinal modes and external cavity modes, rather than from undamped relaxation oscillations, as typically observed in conventional semiconductor lasers. Furthermore, we examine the evolution of the system's dynamics as a function of feedback strength, demonstrating the onset of photonic chaos at feedback levels two orders of magnitude higher than those required in traditional diode lasers, in agreement with experimental observations existing in the literature. Finally, we assess the correlation dimension of the attractor of the resulting nonlinear dynamics. Beyond fundamental insight, this work introduces the use of ESMBEs as a predictive framework for experimental interpretation and device design, enabling the engineering of QCLs for mid- and long-infrared free-space applications, including high-speed transmission, chaos-based LiDAR, and random number generation.





## I. INTRODUCTION

The study of nonlinear dynamics in the mid-infrared (MWIR) and long-infrared (LWIR) wavelength region has garnered considerable attention in recent years, primarily due to the unique advantages this spectral range offers for free-space telecommunications.[1,2] MWIR and LWIR wavelengths are particularly significant due to their reduced vulnerability to degradation under adverse weather conditions compared to near-infrared wavelengths, as well as their enhanced stealth capabilities. These attributes make the MWIR and LWIR regions increasingly compelling for free-space optical systems operating within atmospheric transparency windows. MWIR and LWIR wavelengths are gaining attention for enabling emerging applications such as secure and private communication,[3] LiDAR, and physical random number generation, alongside ongoing advances in high-speed data transmission. Utilizing chaos-based techniques[4] for such applications involves harnessing aperiodic,

deterministic yet unpredictable signals, which are highly sensitive to initial conditions and system parameters. This approach enables the generation of an effectively infinite number of low cross-correlated signals. The inherent unpredictability of chaotic signals provides a robust security layer, ensuring that even minor variations in physical parameters can lead to significantly different outcomes. By exploiting the chaos generated by semiconductor lasers,[5] it is possible to establish secure communication channels with enhanced protection against interception and unauthorized decryption.

Over the past four decades, extensive research has focused on unraveling the physical mechanisms underlying nonlinear dynamics and optical chaos in near-infrared class B[6] interband laser diodes, often through external perturbations such as optical injection or feedback. In conventional laser diodes, the amplification of the relaxation frequency with increasing feedback power is a primary cause of laser instability.[6] Much of the experimental research on mid- and long-infrared and THz nonlinear dynamics has concentrated on quantum cascade lasers (QCLs).[7] QCLs are particularly promising for free-space, high-speed, short-range communications due to their ability to operate in the terahertz frequency range. Moreover, QCLs demonstrate intriguing nonlinear dynamics when exposed to external perturbations. QCLs are categorized as quasi-class-A[6] lasers due to the picosecond timescale for gain recovery and the absence of relaxation oscillations.[8] The absence of relaxation oscillations suggests that QCLs may possess a broad direct modulation bandwidth, potentially extending to several tens of gigahertz. However, experimental observations have so far indicated much smaller bandwidth for direct modulation, raising questions about QCL stability and underscoring the limited understanding of their dynamical properties. Moreover, the short carrier lifetimes in QCLs facilitate the emergence of complex multimode dynamics and contribute to instabilities. Indeed, multimode regimes in QCLs have received significant attention due to their susceptibility to instabilities characteristic of multiple longitudinal mode QCLs.[9] These instabilities are primarily driven by nonlinear physical mechanisms, such as fast spatial hole burning (SHB) and non-zero linewidth enhancement factor (LEF). We define fast SHB as the population grating induced by the standing-wave pattern in the laser cavity.[10] Accurate modeling of QCL behavior is, therefore, crucial for predicting the performance of these semiconductor sources. Given that optical communication systems require dynamic single-mode lasers with narrow linewidths to enhance data transmission rates, this work provides a comprehensive investigation into the nonlinear mechanisms of distributed-feedback (DFB) QCLs in the presence of external optical feedback (EOF). In our previous research,[10] we demonstrated the significant impact of fast SHB and non-zero LEF in shaping the multimode behavior of DFB QCLs, revealing their dynamics to be substantially more diverse compared to class B laser diodes.[11] In this study, we utilize the Effective Semiconductor Maxwell–Bloch Equations (ESMBEs) formalism to model the dynamics of the QCL, treating it as a distributed bidirectional resonator. ESMBEs were initially introduced for the Fabry–Perot (FP) cavity in Refs. 12 and 13. In Ref. 10, ESMBEs were extended in the framework of coupled-mode theory[14] to simulate the effects of a distributed-feedback grating. Additional details of the model are provided in the supplementary material. In the current work, ESMBEs are further extended to incorporate the impact of EOF. This extension follows the methodology outlined in Ref. 15, which examines the onset of frequency combs in the presence of optical feedback in FP QCLs. In particular, following the approach in Ref. 10, we simulate the behavior of a DFB QCL emitting at 9.34 $\mu$m to replicate the characteristics of the experimental DFB QCL under investigation. Building on our previous research,[10] this paper pursues two primary objectives. First, we investigate the fundamental factors limiting the intrinsic direct modulation capabilities of QCLs in the absence of an external target, validating existing experimental and numerical findings from the literature while employing a more comprehensive theoretical framework. Second, we explore the nonlinear behavior of DFB QCLs under EOF, with a particular focus on identifying the mechanisms driving destabilization, the transition to chaos, and the fundamental distinctions between QCLs and class-B diode lasers. In particular, we examine the critical roles of feedback strength, fast SHB, and non-zero LEF, providing a quantitative assessment of the dimension of the attractors through the evaluation of the correlation dimension. In particular, we examine the critical roles of feedback strength, fast SHB, and non-zero LEF, providing a quantitative assessment of the dimension of the attractors through the evaluation of the correlation dimension. While the ESMBEs are an established formalism, their application here to a realistic DFB configuration under EOF enables a detailed investigation of the conditions leading to chaos in QCLs. Our motivation stems from the rising interest in chaos-enabled free-space optical technologies. By deepening the theoretical understanding of chaos onset in MWIR and LWIR QCLs, this study provides valuable insight for future experimental implementations targeting secure communication, LiDAR, and random number generation. Furthermore, the adoption of a distributed-resonator-based model that accounts for the QCL's longitudinal modes allows us to identify significant experimental limitations associated with mid- and long-infrared detectors and oscilloscopes. Indeed, we outline how these experimental constraints inhibit the resolution of the fastest timescales in the system's nonlinear dynamics—particularly those on the order of a picosecond—which are, nevertheless, captured in our simulations. As a result, we prove that experimental characterization of nonlinear behavior remains incomplete, preventing a full description of the complex dynamics exhibited by QCLs under EOF. To the best of our knowledge, this study is the first of its kind, representing a significant advancement in the field.

## II. INTENSITY MODULATION RESPONSE (IMR)

A distinctive feature of QCLs is the absence of relaxation oscillations in their electrical modulation response, attributed to the short carrier lifetime relative to the photon lifetime.

Initial studies suggested that QCLs could theoretically achieve terahertz-level direct intensity modulation bandwidths due to their very short carrier lifetimes as compared to photon lifetime, based on a second-order intensity modulation response (IMR) typically used for interband lasers.[16,17]

In contrast, Ref. 18 analytically solved coupled Langevin rate equations to compute the direct current modulation response. This study concluded that the maximum 3-dB bandwidth is limited by the inverse of the photon lifetime, as this is the longest time constant in QCLs. Similarly, the photon lifetime is responsible for the overdamped modulation response, peculiar to QCLs. As in standard interband laser diodes, it has been observed that at low bias currents, the 3-dB frequency increases with current. At higher bias currents, it

**TABLE I.** Material and device parameters used in simulations for the QCL in the DFB configuration.

| Physical parameters | | Geometrical parameters | | Simulation duration and time step | | Spatial discretization parameters | |
|---|---|---|---|---|---|---|---|
| $\tau_e$ (ps)[13,23,24] | 1 | $R_{\text{front}}$[a] | 32% | $T_{\text{sim}}$ ($\mu$s) | 10 | $\Delta z$ ($\mu$m) | 2.73 |
| $\tau_d$ (fs)[23–25] | 320 | $R_{\text{back}}$[a] | 99% | $\Delta T$ (fs) | 30 | $N_z$ | 734 |
| $\Gamma_c$ | 0.127 | L (mm)[a] | 2 | | | | |
| $f_0$ ($\mu$m$^3$)[13] | $1.1 \times 10^{-7}$ | $V$ ($\mu$m$^3$)[13] | 2240 | | | | |
| LEF[26,27] | 1.2 | $\kappa_{\text{DFB}}$ (cm$^{-1}$)[b] | 9 | | | | |
| $\eta_i$[28] | 85% | | | | | | |
| $\alpha_{\text{tot}}$ (cm$^{-1}$)[29] | 8.9 | | | | | | |
| $\lambda_0$ ($\mu$m)[a] | 9.34 | | | | | | |

[a]Parameters from the vendor's specifications.
[b]Parameters extracted from measurements.

saturates at a value approximated by $f_{-3\,\text{dB}} \approx 1/(2\pi\tau_p)$, concluding that the bandwidth is limited to tens of gigahertz.

Experimental work supports these findings. An 8-$\mu$m QCL was reported to have no relaxation oscillation resonance and a maximum modulation bandwidth of 10 GHz.[19] Similarly, terahertz QCLs have achieved modulation bandwidths of 13 and 24 GHz in test bench studies.[20,21] Both numerical and experimental studies have shown that the direct modulation bandwidth of a QCL is influenced by factors such as the number of periods and the electron extraction time, which is the time required for electrons to traverse the multiple periods of the QCL stack.[22]

In this paper, we evaluate the intrinsic IMR of a DFB QCL emitting at 9.34 $\mu$m in the framework of the ESMBEs formalism. Simulation parameters are listed in Table I. A comprehensive description is provided in the supplementary material. Following the presentation of the simulation results, we will discuss and compare these findings with previous literature. It is worth noting that extrinsic limitations imposed by the equivalent electrical circuit of the packaged device—such as contact geometry, parasitic capacitance, and bias network design—are not included in our current model. Our results, therefore, clarify the upper bounds imposed by the laser's internal dynamics alone. In this context, the term "intrinsic IMR" refers specifically to the modulation response arising from the carrier–photon interaction within the active region, excluding any extrinsic circuit-related effects.

To determine the 3-dB bandwidth from our numerical simulations, we perform a small-signal analysis, according to Eq. (1). The IMR of the QCL is analyzed by introducing a small current step $\delta I_0$ in the injection current and observing the resulting fluctuations $\delta P(t)$ in the optical output power. Additional information on the mathematical derivation of the formula used to numerically estimate the IMR is provided in the supplementary material,

$$IM(\omega) = \frac{1}{\delta I_0} \mathscr{F}\left\{\frac{d\delta P(t)}{dt}\right\}. \tag{1}$$

Figures 1(a)–1(c) illustrate our simulation results. The dashed lines indicate the results obtained by numerically setting fast SHB to zero, as done in Ref. 10. While fabricating a real device with negligible fast SHB is not physically possible, these calculations highlight one of the mechanisms limiting the direct modulation bandwidth of QCLs. When fast SHB is included in the model, single-mode operation is maintained for $I_{\text{th}} \le I_{\text{bias}} \le 1.22 \times I_{\text{th}}$, with an estimated 3-dB bandwidth of ~5.2 GHz at $I_{\text{bias}} = 1.22 \times I_{\text{th}}$. We find a consistent trend with Refs. 18 and 30: at low bias currents, the 3-dB frequency increases with current, but at higher bias currents, it tends to saturate until the device transitions to multimode operation.

In contrast, when fast SHB is numerically set to zero, the frequency range over which the laser maintains single-mode emission broadens significantly, indicating that SHB contributes to mode competition and narrows the stable single-mode operating range. Under this condition, single-mode emission persists up to $I_{\text{bias}} = 1.70 \times I_{\text{th}}$, yielding a maximum 3-dB bandwidth of ~11.6 GHz—almost double that observed when fast SHB is included in the model. This suggests that omitting fast SHB in numerical

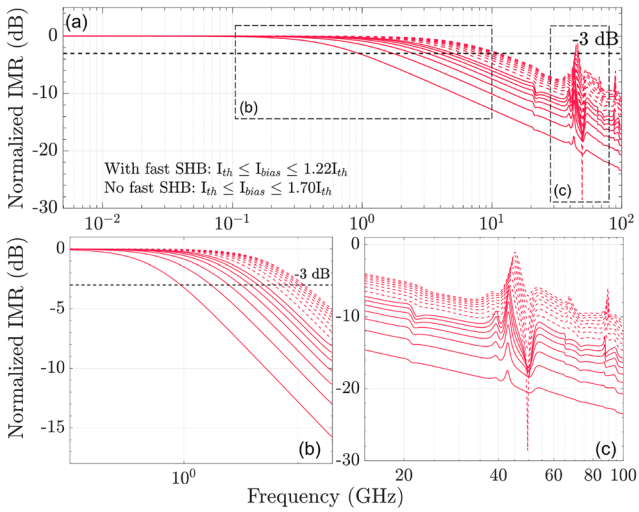


**FIG. 1.** (a) Normalized IMR obtained varying $I_{\text{bias}}$ in the frequency range [0, 100] GHz. Solid line: including fast SHB and dashed line: excluding fast SHB. (b) Zoom of the IMR in the frequency range [0, 10] GHz. The absence of relaxation oscillations is particularly evident. (c) Zoom of the IMR in the frequency range [15, 100] GHz. The PPR resonance is here emphasized.

models overestimates the maximum modulation bandwidth of mid- and long-infrared QCLs.

In both cases, a pronounced peak around 44 GHz is observed, which corresponds to photon–photon resonance (PPR).[31] This resonance results from interactions between the lasing mode and a competing longitudinal mode. Although relaxation oscillations are fully damped in QCLs, the longer internal cavity length compared to conventional diode lasers (1–10 mm vs 200 $\mu$m–3 mm) enhances the likelihood of mode competition, particularly as $I_{\text{bias}}$ increases. This indicates that mode competition could further constrain the maximum 3-dB bandwidth for direct modulation of DFB QCLs. Despite the absence of traditional relaxation oscillations, the presence of PPR could be exploited to improve the modulation response of QCLs at specific high frequencies, which is crucial for applications requiring large bandwidths. These findings underscore the importance of fast SHB and PPR in determining QCL modulation characteristics, providing valuable insights for optimizing these lasers for high-speed communication and advanced photonic applications.

In contrast to the model presented in Ref. 18, we incorporate the nonlinear physical effects of SHB and LEF. We confirm that the modulation bandwidth of QCLs is limited to tens of gigahertz, since our numerical simulations show a bandwidth of ~5.2 GHz. Nevertheless, we do not attribute this limitation solely to the photon lifetime, because if we were to follow the approach in Ref. 18, the maximum 3-dB bandwidth would be ~4.1 GHz. In addition, we have demonstrated that one primary mechanism limiting the QCL's modulation bandwidth is fast SHB. Furthermore, unlike previous models, our simulations account for photon–photon resonance and do not assume single-mode operation, thereby incorporating spatial effects within the laser cavity. This approach allows us to show that the interplay between competing longitudinal modes is a key factor in determining the QCL's IMR. Similar to photon lifetime, the interaction of longitudinal modes is strongly influenced by the QCL's geometrical parameters, including the internal cavity length, the use of high-reflectivity/anti-reflectivity coatings at the laser's facets, and the grating coupling strength $k_{\text{DFB}}$. Additional details on the impact of these factors are provided in the supplementary material. This explains why our model yields results that are in close agreement with those of Refs. 18 and 30, while providing deeper insight into the role of longitudinal mode competition in shaping the QCL's modulation characteristics.

## III. EXTERNAL OPTICAL FEEDBACK (EOF)

Experimentally, various dynamic behaviors have been observed in numerous types of semiconductor lasers in the presence of EOF, including instability, bistability, self-pulsations, and coherence-collapse (CC) states.[32] The term "coherence collapse" was introduced by Lenstra and colleagues in 1985.[33] Numerical simulations demonstrated that under very high feedback ratios, the interaction between phase and amplitude results in linewidth enhancement and a significant reduction in coherence length compared to the free-running case, aligning well with experimental observations. The relationship between chaos and the CC regime was experimentally established through analyses of the radio frequency (RF) spectrum of lasers, which corresponded with the power spectral density obtained from numerical simulations.[34] Generally, CC dynamics are characterized by a broad RF spectrum, with the upper frequency limit often related to the intrinsic relaxation frequency, particularly in near-infrared lasers. Following the extensive studies on deterministic chaos in various semiconductor lasers during the 1980s and 1990s,[35–38] extending these concepts to QCLs became pertinent due to their mid- and long-infrared emission wavelengths[39–41] not addressable by near-infrared and visible-light semiconductor lasers. The first demonstration of chaos in mid- and long-infrared DFB QCLs was reported in Ref. 42, although these initial results were left unexplained. The observed nonlinear dynamics were confined to conditions near the threshold current under quasi-continuous bias at room temperature. Subsequently, in Ref. 43, the authors provided a detailed description of the conventional nonlinear dynamics of DFB QCLs in an external-cavity configuration, observing phenomena including external-cavity frequency oscillations, period-doubling oscillations, low-frequency fluctuations (LFFs), and CC dynamics. Typically, these dynamics emerge sequentially with increasing feedback strength, although restabilization events can disrupt this order. Hereafter, we demonstrate the observation of dynamics equivalent to those of experimental findings in Ref. 43 and provide further insights by overcoming certain experimental limitations. For the first time, we elucidate the complex dynamics of QCLs under EOF, revealing that the origin of nonlinear dynamics in QCLs fundamentally differs from that in diode lasers.[9] Moreover, the nature of coherence collapse in chaotic QCL time traces is distinct from that observed in conventional lasers. While existing concepts developed for semiconductor lasers remain applicable to QCLs, our results indicate the necessity for their reinterpretation in this context.

### A. Theoretical model

The Lang–Kobayashi (LK)[44] model has provided foundational insights into the dynamics of semiconductor lasers under external optical feedback, capturing many hallmark phenomena—such as coherence collapse and low-frequency fluctuations—in weak- and moderate-feedback regimes. Nevertheless, its point-like, single-mode formulation might leave out mechanisms that become decisive whenever the mutual interaction of multiple internal longitudinal modes dominates the dynamics.

As we will demonstrate in this research, this is particularly the case for QCLs, where the interplay between internal longitudinal modes—promoted by SHB and non-zero LEF—plays a critical role in enabling feedback-induced instabilities. Neglecting these effects may result in failing to capture the onset of complex dynamical regimes, including chaos. Indeed, simulations that rely solely on the LK formalism predict undamped relaxation oscillations and long-term ultrastability in mid-IR and THz QCLs[9]—features that contrast with experimental observations of feedback-induced quasi-periodicity and chaotic emission.[42,43]

By self-consistently linking the spatiotemporal evolution of the optical field to carrier and polarization dynamics, the ESMBEs naturally include linewidth-enhancement, spatial hole-burning, and frequency-dependent gain dispersion—ingredients that are essential for reproducing comb formation, multimode instabilities, and chaotic regimes in QCLs. The model considers two counterpropagating fields, $E^+$ and $E^-$, representing, respectively, the forward and backward waves, propagating either in the DFB or in the external cavity along the longitudinal direction $z$.

In particular, we consider an external reflector located at a distance $L_{ext}$ from the right facet of the QCL, with a frequency-independent reflectivity $r_{ext}$. Here, $\varepsilon_L$ quantifies the total losses experienced by the field in the external cavity, and $\varepsilon_S$ quantifies the losses due to re-injection. The field emitted by the QCL propagates in the external cavity, is reflected by the target, and is partially re-injected into the laser cavity. If we define $\varepsilon = r_{ext}\varepsilon_L\varepsilon_S$, the optical field re-injected at the DFB facet in $z = L$ and facet reflectivity $R_{front}$ can be expressed as follows:

$$E^-(L,t) = \sqrt{R_{front}}E^+(L,t) + \varepsilon t_L^2 E^+(L,t-\tau_{ext})e^{-i\omega_0\tau_{ext}}, \quad (2)$$

$$E^+(0,t) = \sqrt{R_{back}}E^-(0,t), \quad (3)$$

where $L$ is the length of the QCL cavity, $R_{front} \in \mathbb{R}$ is the power reflectivity of the QCL's front facet, $R_{back} \in \mathbb{R}$ is the power reflectivity of the QCL's back facet, $t_L = \sqrt{1-R_{front}}$ is the transmissivity of the laser facet for both the outgoing and incoming fields, $\omega_0$ is the central angular frequency, and $\tau_{ext} = 2L_{ext}/c$ is the round trip time in the external cavity. The feedback is incorporated through the additional term on the right-hand side of Eq. (1). The ratio between the feedback power and the output power is given by $\varepsilon^2$.

## B. Numerical results

The simulation parameters are detailed in Tables I and II. The bias current is set to $I_{bias} = 1.07 \times I_{th}$, which corresponds to a case of single-mode emission in free-running operation.

As an initial step in the analysis, we examine the influence of the feedback strength ($\varepsilon^2$). An external cavity length of $L_{ext} = 25$ cm is chosen to replicate a typical experimental configuration, corresponding to the long-cavity regime, where the free-spectral-range (FSR) of the internal cavity and the external cavity frequency ($f_{ext}$) differ by several orders of magnitude.[43] Then, we compare the numerical results with the experimental results of Ref. 43. It is important to note that varying the feedback strength from 0% to 100% is difficult to achieve in a laboratory setting because the splitting ratio of the beam splitter utilized to realize the external cavity is typically fixed. Moreover, fabricating beam splitters with very asymmetric splitting ratios is costly. Similarly, achieving short cavities is challenging due to the bulky components involved in mid- and long-infrared EOF setups, such as laser packaging, lenses, beam splitters, and mirrors. We conclude by exploring the influence of the nonlinear physical mechanisms of fast SHB and LEF on the observed nonlinear dynamics.

### 1. Impact of $\varepsilon^2$

The resulting bifurcation diagram is reported in Fig. 2, and describes the evolution of the power extremes (both maxima and minima) extracted from the time series as a function of $\varepsilon^2$. Figure 3 depicts some examples of time traces (and relative optical and RF spectra) at increasing values of $\varepsilon^2$ (i.e., 0%, 3%, 6%, 11%, 30%, 60%, 80%, and 100%), to highlight the features of the observed nonlinear dynamics. The case $\varepsilon^2 = 0\%$ corresponds to the free-running condition.

**TABLE II.** Parameters used in simulations for the DFB QCL in EOF configuration.

| $L_{ext}$ (cm) | $f_{ext}$ (MHz) | $\varepsilon^2$ (%) | $I_{bias}$ (mA) |
|---|---|---|---|
| 25 | 598 | [0, 100] | 320 |

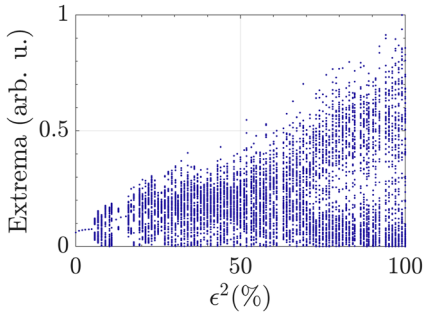


**FIG. 2.** Numerical bifurcation diagram, with parameters of simulations in Tables I and II.

For $\varepsilon^2 \leq 5\%$, the perturbation given by the optical feedback leads to a steady-state, but with higher output power with respect to the free-running operation, as emerges in Fig. 4. Here, during the transient, right after EOF is turned on, it is possible to identify some damped oscillations at the external cavity frequency $f_{ext}$. Experimental evidence of equivalent transient instabilities in single-mode terahertz QCLs confirms our numerical findings.[45] This distinguishes the QCLs from interband lasers, where an external perturbation causes the observation of the intrinsic relaxation frequency, which we have demonstrated in Sec. II to be overdamped in QCLs.

For $\varepsilon^2 \geq 6\%$, destabilization is obtained, with a number of competing longitudinal modes that increases with feedback strength. In addition, we always appreciate the signature of both internal resonances and external cavity frequency, since we are simulating a long-cavity regime condition.

In particular, for $6\% \leq \varepsilon^2 \leq 11\%$, we observe a regime we define as mixed states with periodic behavior on two timescales: the picosecond timescale of the longitudinal modes on the internal laser cavity and a nanosecond timescale, relative to the external cavity frequency components. By looking at the optical spectrum, we observe that each excited mode of the laser cavity presents a fine structure composed of a few secondary peaks around the main one. Meanwhile, in the RF spectrum, we have a sequence of frequency bands whose center frequency corresponds to a multiple of FSR, with secondary peaks spaced by $f_{ext}$. The periodicity can still be appreciated because the number of excited internal longitudinal modes and external modes is small. The time trace in Tiffany color of Fig. 3 is an example of such findings.

In addition, in correspondence with specific values of $\varepsilon^2 \leq 11\%$, we can also observe periodic or aperiodic low-frequency components at a few MHz (corresponding to microsecond timescale), together with the aforementioned timescales. What we observe is a sudden power dropout followed by a gradual power recovery, with pulses that can be more or less regular, according to the value of feedback strength. Because of the similarity of this phenomenon to that observed in other semiconductor lasers and also experimentally in QCLs, we define this regime as the low-frequency fluctuations

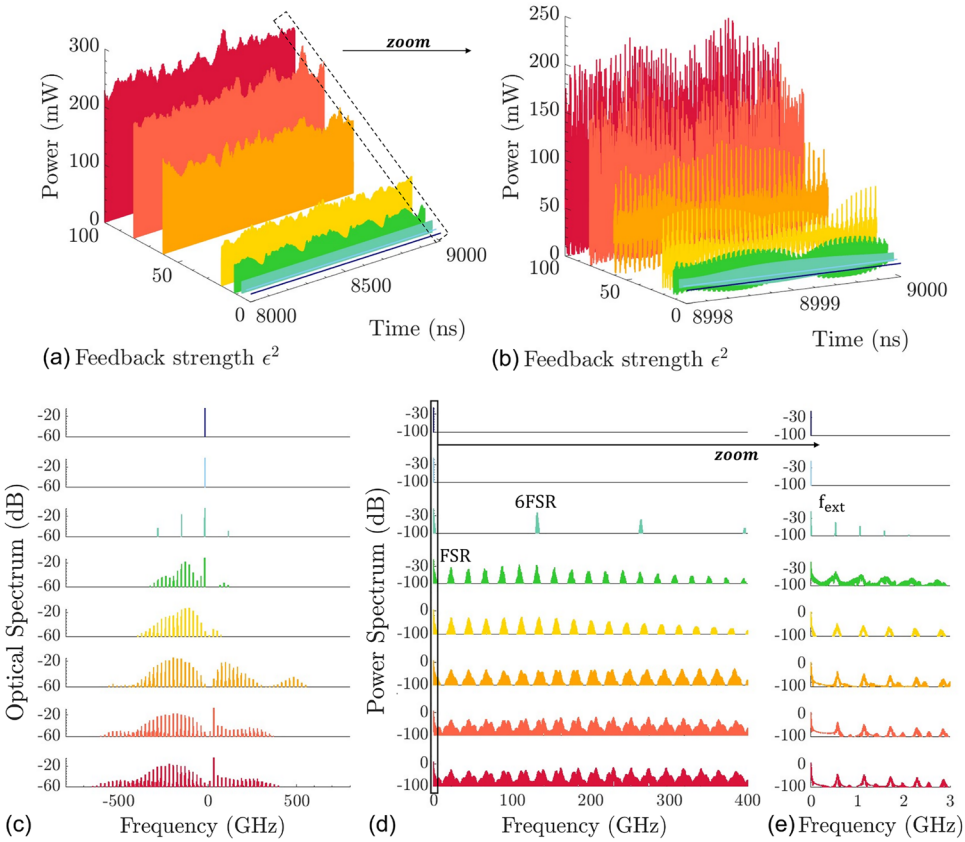


**FIG. 3.** Evolution of time traces toward chaos at 320 mA. (a) Time traces in the temporal window [8000, 9000] ns. (b) Time traces in the temporal window [8998, 9000] ns. (c) Optical spectra. [(d) and (e)] RF spectra. From top to bottom, $\epsilon^2$ assumes the following increasing values: 0%, 3%, 6%, 11%, 30%, 60%, 80%, and 100%.

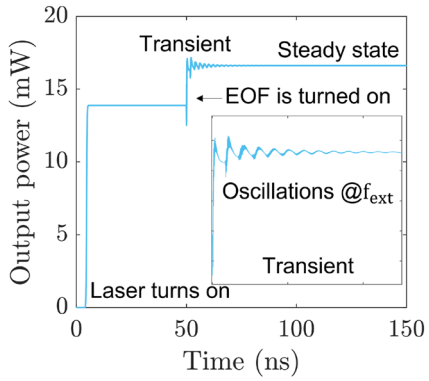


**FIG. 4.** Numerical time trace for a bias of 320 mA, $\epsilon^2$ = 3%, and a temporal window $\Delta t$ = [0, 150] ns. At t = 50 ns, the EOF is turned on. (inset) Zoom in on the transient behavior of the QCL on a temporal window $\Delta t$ = [49, 80] ns, with evident damped oscillations at $f_{ext}$.

regime. The green time trace in Fig. 3 shows that LFF involves multimode dynamics. As in the case of mixed states, the optical spectrum consists of internal longitudinal modes displaying a finer structure composed of secondary peaks at a distance equal to the external cavity frequency. However, as widely reported for other semiconductor lasers, the RF spectrum shows a characteristic frequency on the order of a few MHz. Hence, the term LFF is utilized here to emphasize the strong contribution of low-frequency components. In addition, we recognize that the nature of such dynamics is unique in DFB QCLs and perhaps different from what is observed in conventional diode lasers. In particular, our simulations reveal that the number of modes after each drop changes. Similarly, the dominant modes just after the drop are not the dominant ones just before it, due to the exchange of energy among the modes. The origins of the oscillations can be understood as a partial phase locking between modes.

For 12% $\leq \epsilon^2 <$ 16%, we observe restabilization: the laser operates again in a steady-state regime, even if the observed transient time can be as long as a few $\mu$s. For $\epsilon^2$ = 16%, 17%, we have the mixed state regime.

By increasing the feedback strength in the range 18% $\leq \epsilon^2 \leq$ 100%, an increasing number of internal longitudinal modes and external modes come into play. We can identify this highly multimode regime as chaos, as we will henceforth prove by providing the estimation of one of the main metrics of chaos indicators, specifically the correlation dimension. Figure 3(c) compares the optical spectra obtained for increasing values of $\epsilon^2$. As the feedback strength increases, two asymmetric sidebands are identifiable around the lasing mode. The latter is suppressed for moderate feedback levels. The sidebands broaden as $\epsilon^2$ is increased, but their splitting remains constant. For high feedback levels, a new dominant mode

is identified, but it does not coincide with the main lasing one (it is around 50-GHz distant). What distinguishes mixed states from chaos is the number of excited internal longitudinal modes and external cavity modes. The higher $\varepsilon^2$, the denser the optical and RF spectra. Therefore, our numerical findings extend experimental observations, suggesting that the chaos bandwidth in QCLs is highly multimode and not associated with broad RF spectra, as in conventional diodes.

Figure 5 showcases a series of phase portraits, which are graphical representations used to visualize the behavior of dynamical systems (multimedia available online). In particular, a phase portrait plots the state of a system in a phase space, where each point represents a possible state of the system, and the trajectory shows how the system evolves over time. In this case, the phase portraits are obtained by plotting the electric field amplitude resulting from simulations and its derivative against each other over time. As $\varepsilon^2$ increases, the phase portraits illustrate the changing dynamics of the system. This provides insight into the system's behavior under different feedback conditions.

Figure 5 is supplemented by Table III, presenting the correlation dimension $d$[46] for each analyzed time trace. This metric quantifies the dimension of the system's attractor and measures how a system's dynamics evolve over time and how unpredictable or structured its behavior is. The attractor is defined as the long-term behavior of the system[47] and can take different forms depending on the nature of the dynamics. The methodology employed to determine $d$ is detailed in the supplementary material.

When $\varepsilon^2 = 0\%$, the phase portrait represents a single point in the phase space. This indicates that the QCL is in a steady state. The same reasoning holds for $\varepsilon^2 = 3\%$. Meaningful values of correlation dimension $d$ cannot be extracted for $\varepsilon^2 = 0\%$ and $\varepsilon^2 = 3\%$, as there is no dynamic evolution to analyze.

When $\varepsilon^2 = 6\%$, a limit cycle appears, which is reflected in a relatively low correlation dimension $d = 2.346$, indicating that the attractor is simple and low-dimensional.

With $\varepsilon^2 = 11\%$ and $\varepsilon^2 = 30\%$, the system's dynamics become increasingly more complex: the path is no longer a simple cycle but rather a more convoluted and intricate pattern, reflecting the growing influence of the external feedback and, for $\varepsilon^2 = 11\%$, also of low-frequency contributions. Indeed, the correlation dimension d rises to 3.892 for $\varepsilon^2 = 11\%$ and 3.763 for $\varepsilon^2 = 30\%$. We attribute the slight decrease in $d$ for increasing $\varepsilon^2$ to the absence of dominant low frequency components when $\varepsilon^2 = 30\%$. When $\varepsilon^2 \geq 60\%$, the system transitions into a chaotic regime; in fact, the correlation dimension $d$ rises steadily, reaching ~5.038 for $\varepsilon^2 = 100\%$. This progression highlights that as the feedback strength increases, the system's dynamics become more complex, with trajectories exploring higher-dimensional structures and requiring more degrees of freedom to be accurately described. The corresponding increase in $d$ confirms the presence of a more intricate and space-filling attractor,



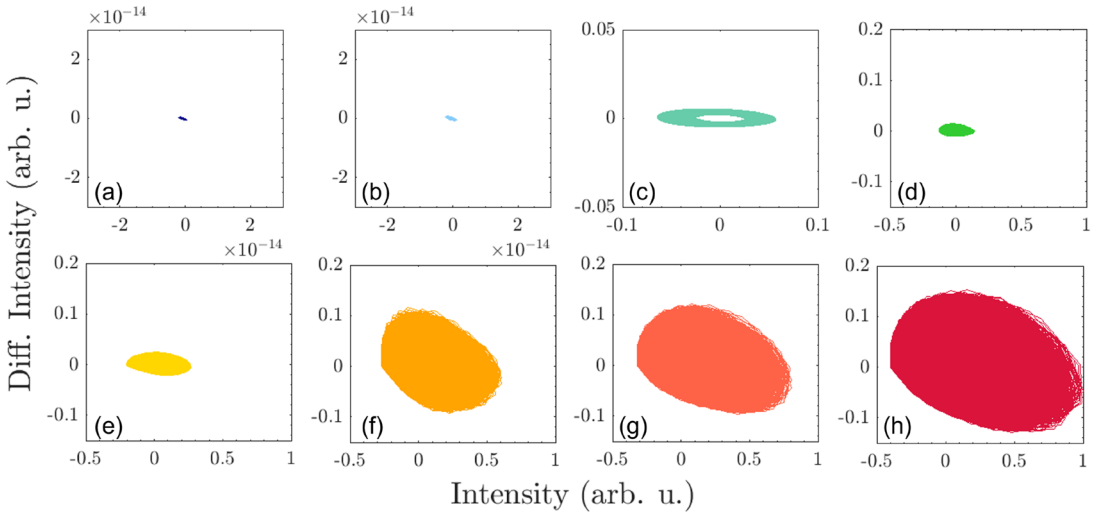


**FIG. 5.** 2D phase portraits of numerical time traces for increasing values of $\varepsilon^2$: [(a)–(h)] 0%, 3% (fixed point), 6% (limit cycle), 11%, 30%, 60%, 80%, and 100% (strange attractor with increasing dimension). (Multimedia available online).http://doi.org/10.1063/5.0252956.1; http://doi.org/10.1063/5.0252956.2

**TABLE III.** Estimation of correlation dimension d for varying feedback strength: $\varepsilon^2 = 0\%, 3\%, 6\%, 11\%, 30\%, 60\%, 80\%, 100\%$.

| $\varepsilon^2$ (%) | 0 | 3 | 6 | 11 | 30 | 60 | 80 | 100 |
|---|---|---|---|---|---|---|---|---|
| $d$ | ⋯ | ⋯ | 2.346 ± 0.015 | 3.892 ± 0.227 | 3.763 ± 0.198 | 4.477 ± 0.207 | 4.912 ± 0.106 | 5.038 ± 0.122 |

characteristic of a well-developed chaotic system. At this stage, the system's dynamics are practically unpredictable over long timescales due to sensitivity to initial conditions, with no discernible periodicity or regularity. This complex trajectory in the phase space goes under the name of a strange attractor.[47]

We can conclude by stating that the investigation of nonlinear dynamics in DFB QCLs under EOF reveals intriguing phenomena that extend concepts traditionally applied to diode lasers, although with distinct interpretations. Using the ESMBEs, our study demonstrates that destabilization in DFB QCLs is driven by underdamped oscillations at the external cavity frequency $f_{ext}$, which, in contrast to conventional diode lasers, occurs with a feedback strength approximately two orders of magnitude greater.[9] Indeed, in standard diodes, destabilization is related to the relaxation oscillation frequency (generally in the order of a few GHz). In QCLs, the presence of an external target induces a complex interplay between internal longitudinal modes and external cavity modes, resulting in multimode behavior characterized by mixed states, the potential emergence of low-frequency components, and chaos as feedback strength increases. Notably, chaos is observed as a highly multimode phenomenon in DFB QCLs, distinct from conventional semiconductor lasers, where linewidth broadening typically indicates such transitions. This feature is particularly promising for application purposes since the spacing of each frequency band is tunable with continuity by varying $L_{ext}$, and at the same time, the central frequency can be chosen between the excited longitudinal modes of the QCL cavity. For instance, remaining in the field of communication, they could be appealing for the implementation of novel multi-channel communication systems.

### 2. Comparison with experimental results

Currently, the numerical results do not fully align with experimental observations in Ref. 43 because of the different order of magnitude observed in the timescale of the QCL's nonlinear dynamics. In fact, the fine resolution of our numerical simulations reveals the smaller timescale to be on the picosecond order. However, the absence of high-speed mid- and long-infrared detectors in the experimental findings of Ref. 43 limited the resolution to the nanosecond timescale, thus limiting definitive conclusions regarding the presence of driving frequencies and the bandwidth of nonlinear dynamics. Indeed, the current detectors and oscilloscopes, which are bandwidth-limited in the mid- and long-infrared, prevent us from observing the high-frequency components related to the FSR and its multiples, rendering the picosecond timescale not observable. Consequently, we can only detect dynamics on the microsecond and nanosecond timescales. Hence, to enable a fair comparison with the experiments reported in Ref. 43, we applied a low-pass Butterworth filter to the numerical results, with a cutoff frequency of 700 MHz, matching the cutoff frequency of the mercury cadmium telluride (MCT) detector used in those experiments. Under these conditions,

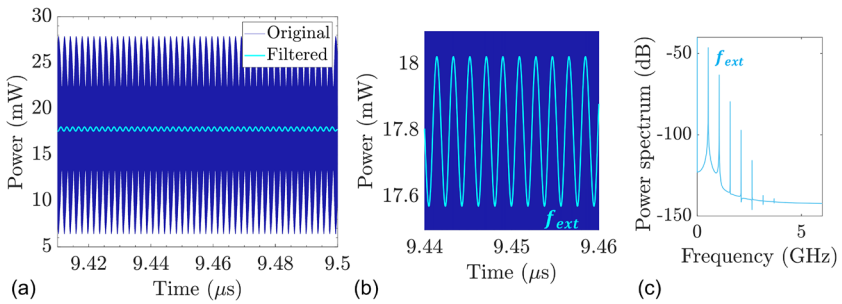


**FIG. 6.** Results from simulations for a bias of 320 mA and $\varepsilon^2 = 6\%$. [(a) and (b)] Time trace (blue) before and (light blue) after the application of numerical low-pass filtering. (c) RF spectrum limited to a low-frequency range ([0, 6] GHz). $f_{ext}$ signature is evident.

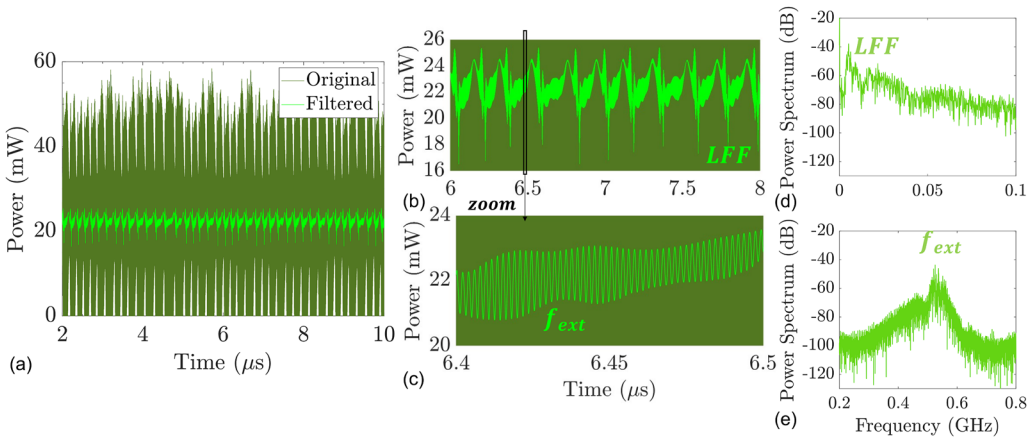


**FIG. 7.** Results from simulations for a bias of 320 mA and $\varepsilon^2 = 11\%$. [(a)–(c)] Time trace (dark green) before and (light green) after the application of numerical low-pass filtering. [(d) and (e)] RF spectrum limited to a low-frequency range ([0, 0.7] GHz). LFF and $f_{ext}$ features are evident.

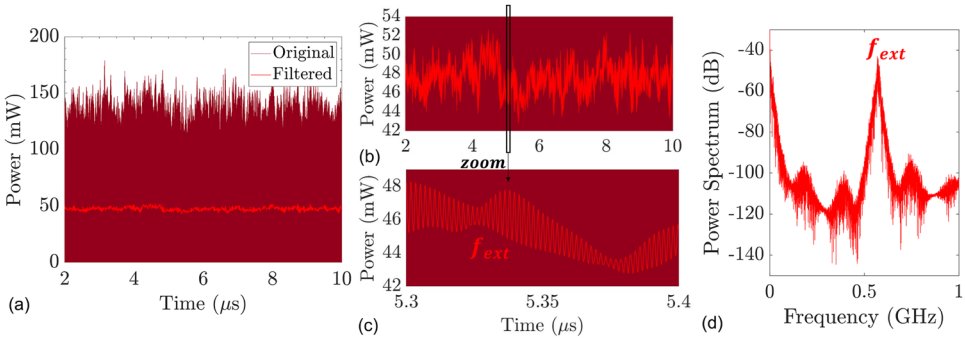


**FIG. 8.** Results from simulations for a bias of 320 mA and $\varepsilon^2$ = 60%. [(a)–(c)] Time trace (dark red) before and (red) after the application of numerical low-pass filtering. (d) RF spectrum limited to a low-frequency range ([0, 1] GHz). $f_{ext}$ signature is evident.

we found good agreement between the numerical results and the experimental data of Ref. 43.

Notably, the periodic mixed states appeared as sinusoidal waves oscillating at the external cavity frequency, as emerges from Fig. 6. In both simulations and experiments (Figs. 3–5 of Ref. 43), we observed that the measured external cavity frequency value was slightly lower than the nominal value, with the observed frequency at 520 MHz instead of the expected 600 MHz. This discrepancy has been previously reported in QCLs.[48]

The transition to chaotic behavior occurs when LFFs are observed. The LFF pattern in QCLs exhibits a maximum frequency of a few dozen MHz with a broad low-frequency component [see the RF spectrum in Fig. 7(d)]. However, the contribution of the external cavity remains present, both in numerical simulations and experimental findings,[43] as illustrated in Fig. 7(e). Finally, chaos is observed when $\varepsilon^2$ is further increased. Figure 8 reports an example for $\varepsilon^2$ = 60%, which is still possible to reproduce in a laboratory environment.

### 3. Impact of fast SHB

In Ref. 10, we demonstrated that fast SHB plays a pivotal role in shaping the dynamics of a QCL. Similarly, in Sec. II of this paper, our numerical results show that fast SHB is crucial for accurately estimating the modulation bandwidth of a QCL. This section confirms the importance of fast SHB for shaping the QCL's nonlinear behavior: Fig. 9 is generated by following the same procedure as in Fig. 2, but with fast SHB numerically set to zero. Figure 9 further illustrates that when fast SHB is set to zero in our model, the QCL exhibits more stable behavior compared to the one shown in Fig. 2. Indeed, the QCL becomes destabilized only at a feedback strength of $\varepsilon^2$ = 25%, which is five times higher than the destabilization threshold previously observed when SHB is not neglected. For feedback strengths greater than 25%, the laser dynamics transition into a multimode regime, although intermittent single-mode operation persists, even at high feedback strengths (around 90%). The evaluation of the correlation dimension $d$ for $\varepsilon^2$ = 100% indicates that the chaotic dynamics exhibit relatively low complexity, as $d \approx 3.774$. This value is more than one unit lower compared to the same conditions when SHB is included. This behavior is attributed to the fact that fast SHB is a physical phenomenon that induces nonlinear dynamics in the QCL. When fast SHB is set to zero, the laser is able to maintain stable single-mode operation at much higher feedback strengths, as the absence of SHB prevents the onset of the mode-competition effect typically associated with it. Consequently, the QCL appears more stable under feedback conditions that would otherwise lead to multimode operation.

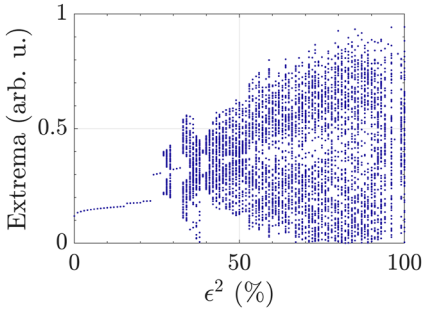


**FIG. 9.** Numerical bifurcation diagram with parameters of simulations in Tables I and II, by forcing fast SHB to zero.

### 4. Impact of LEF

QCLs are well-known for their relatively small LEF. In this paragraph, we inspect the influence of LEF. Figure 10(a) represents the resulting bifurcation diagram, setting the parameters of simulations as reported in Tables I and II. $\varepsilon^2$ = 30% to observe more diversified dynamics while varying the LEF with a step of 0.1 between 0 and 2. In addition, $\varepsilon^2$ = 30% and $L_{ext}$ = 25 cm are conditions still reproducible in an experimental environment.

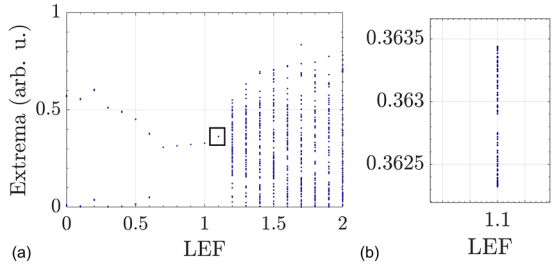


**FIG. 10.** Numerical bifurcation diagram with parameters of simulations in Tables I and II, (a) by varying LEF from 0 to 2 with a step of 0.1. (b) Zoom on LEF = 1.1, to highlight the QCL's periodic behavior.

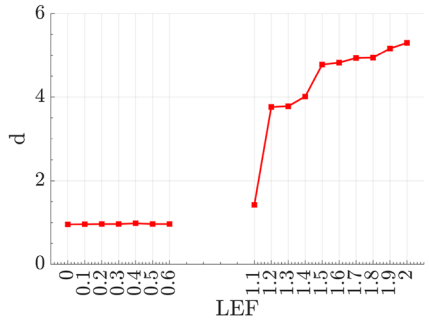


**FIG. 11.** Estimation of correlation dimension $d$ for varying values of LEF: LEF is comprised of numbers between 0 and 2 with a step of 0.1.

The bifurcation map displays an increasing nonlinearity with increasing LEF, since the chaos is observed only when LEF > 1.1. For 0 ≤ LEF ≤ 1.1, the contribution of external cavity modes is absent, and we mainly identify harmonic states when 0 ≤ LEF ≤ 0.6 and single-mode behavior when 0.7 ≤ LEF ≤ 1. Harmonic behavior appears again for LEF = 1.1, as highlighted in Fig. 10(b). Figure 11 reports the evaluation of the correlation dimension $d$ for varying values of LEF, as outlined in the supplementary material. In case of steady-state behavior, no meaningful $d$ can be retrieved. If 0 ≤ LEF ≤ 0.6, the dynamics is periodic, and no external frequency components come into play. Therefore, we obtain a correlation dimension that is approximately around 1. The same reasoning applies for LEF = 1.1. If LEF ≥ 1.2, the behavior is chaotic, with an increasing attractor's dimension, underlined by the increasing correlation dimension $d$ of nearly 5.302 when LEF = 2.

Our results are consistent with the numerical findings derived from the application of the LK model in Ref. 49, extending them to the case of a realistic DFB QCL. A possible explanation resides in the physical meaning of LEF itself. A small LEF corresponds to a weak field amplitude-phase coupling, supporting at most harmonics within the internal cavity but suppressing the contribution of the external cavity, concurring in destabilizing the QCL. When LEF ≥ 1.2, the amplitude-phase coupling is high enough to destabilize the laser, facilitating highly multimode behavior, where both external and QCL's longitudinal modes contribute to the dynamics' nonlinearity.

To conclude, the goal of this paragraph is to underline the key role of non-zero LEF as an additional nonlinear phenomenon—adding up to fast SHB—in contributing to the destabilization of the theoretically ultra-stable QCL. In particular, our findings demonstrate that only appropriately high values of LEF can explain the experimental observations of nonlinear dynamics—and consequently chaos—in DFB QCLs under EOF.

## IV. CONCLUSIONS

This study is a pioneering work in the context of ESMBEs formalism to compute the intrinsic IMR of DFB QCLs. Indeed, by incorporating the nonlinear physical effects of fast SHB and LEF, we have demonstrated that the intrinsic IMR is limited to tens of gigahertz, where the term "intrinsic" refers exclusively to the modulation response arising from carrier–photon interactions within the active region, excluding any extrinsic circuit-related effects. This limitation is not solely attributed to the photon lifetime but especially to the interplay between competing longitudinal modes. Both the photon lifetime and the interaction of longitudinal modes are strongly affected by geometrical parameters, such as the internal cavity length or the facets' reflectivities. Hence, design choices are critical for the QCL's bandwidth enhancement.

Furthermore, our analysis explores the nonlinear dynamics of DFB QCLs under EOF influence. The generation of photonic chaos in QCLs requires feedback strengths exceeding those of conventional lasers by at least two orders of magnitude. This highlights the distinct nature of QCLs, where chaos emerges not from undamped relaxation oscillations but from the interplay between internal longitudinal cavity modes and external cavity modes. The present study is carried out within the ESMBEs framework, which enables a physically consistent modeling of QCL dynamics by capturing both the internal longitudinal modes and external modes interactions and spatially dependent effects—such as spatial hole burning—that play a central role in the emergence of nonlinear dynamics. It is important to emphasize that the aim of this work is not to introduce a new modeling formalism but to employ the ESMBEs as a physically grounded tool to interpret the complex nonlinear dynamics of QCLs under EOF. By applying this framework to a realistic DFB QCL, we provide a deeper understanding of the mechanisms leading to chaos—an essential step toward identifying the operating conditions and device parameters that enable the development of chaos-based free-space optical applications.

Through our simulations, we have thoroughly investigated the impact of the feedback strength $\varepsilon^2$ on the observed nonlinear dynamics, quantifying the system's chaotic behavior through the evaluation of the correlation dimension. In addition, we have proved that fast SHB is one of the primary causes of destabilization in QCLs, which would otherwise exhibit higher stability. Similarly, we have established that a LEF of zero or near zero fails to replicate the experimentally observed behavior in simulations. This finding further supports the notion that the LEF in QCLs cannot be null, as theoretically predicted.

Looking ahead, technological advancements in detectors and oscilloscopes with broader bandwidths will allow us to explore behavior at GHz frequencies, enabling us to distinguish contributions from internal longitudinal modes. In particular, it is critical to investigate the key factors that influence the characteristics of photonic chaos, with a focus on expanding the chaos bandwidth. A broader chaos bandwidth is directly linked to the rate of encrypted communication, highlighting its significance for secure communication systems. Future research should prioritize these critical parameters to enhance chaos bandwidth and improve the performance of secure communication technologies.

## SUPPLEMENTARY MATERIAL

The supplementary material provides a detailed description of the model underlying our numerical results, beginning with the ESMBEs initially introduced for a FP cavity. It then outlines the procedure used to incorporate the DFB grating into the model, followed by the modifications required to account for the presence of an external target. Subsequently, we present the mathematical

derivation of the formula employed in our study to numerically compute the IMR. Additional analyses are introduced to examine the parameters that have the greatest impact on the −3 dB modulation bandwidth. Finally, we introduce the procedure used to determine the correlation dimension of the time series analyzed in the paper and provide two graphical examples to illustrate the results.

## ACKNOWLEDGMENTS

The authors acknowledge Professor Damien Rontani from the University of CentraleSupélec for his support in the evaluation of the correlation dimension. This work was supported by the Direction Générale de l'Armement (DGA) and the European Office of Aerospace Research and Development (Grant No. FA8655-22-1-7032).

## AUTHOR DECLARATIONS

### Conflict of Interest

The authors have no conflicts to disclose.

### Author Contributions

**S. Zaminga**: Conceptualization (lead); Data curation (lead); Formal analysis (lead); Investigation (lead); Methodology (lead); Software (lead); Writing – original draft (lead); Writing – review & editing (lead). **L. Columbo**: Conceptualization (supporting); Investigation (supporting); Methodology (supporting); Supervision (equal); Validation (equal); Writing – review & editing (equal). **C. Silvestri**: Visualization (equal); Writing – review & editing (supporting). **M. Gioannini**: Supervision (equal); Validation (equal); Visualization (equal); Writing – review & editing (equal). **F. Grillot**: Supervision (equal); Validation (equal); Visualization (equal); Writing – review & editing (equal).

## DATA AVAILABILITY

The data that support the findings of this study are available from the corresponding author upon reasonable request.

## REFERENCES

[1] V. W. S. Chan, "Free-space optical communications," J. Lightwave Technol. **24**, 4750–4762 (2006).
[2] M. A. Khalighi and M. Uysal, "Survey on free space optical communication: A communication theory perspective," IEEE Commun. Surv. Tutorials **16**, 2231–2258 (2014).
[3] P. Didier, S. Zaminga, O. Spitz *et al.*, "Data encryption with chaotic light in the long wavelength infrared atmospheric window," Optica **11**, 626–633 (2024).
[4] M. Li, Y. Hong, Y. Song, and X. Zhang, "Effect of controllable parameter synchronization on the ensemble average bit error rate of space-to-ground downlink chaos laser communication system," Opt. Express **26**, 2954–2964 (2018).
[5] M. Sciamanna and K. A. Shore, "Physics and applications of laser diode chaos," Nat. Photonics **9**, 151–162 (2015).
[6] D. M. Kane and K. A. Shore, *Unlocking Dynamical Diversity: Optical Feedback Effects on Semiconductor Lasers* (John Wiley & Sons, 2005).
[7] J. Faist, F. Capasso, D. L. Sivco, C. Sirtori, A. L. Hutchinson, and A. Y. Cho, "Quantum cascade laser," Science **264**, 553–556 (1994).
[8] F. Capasso, C. Gmachl, D. L. Sivco, and A. Y. Cho, "Quantum cascade lasers," Phys. World **12**, 27 (1999).
[9] F. P. Mezzapesa, L. L. Columbo, M. Brambilla, M. Dabbicco, S. Borri, M. S. Vitiello, H. E. Beere, D. A. Ritchie, and G. Scamarcio, "Intrinsic stability of quantum cascade lasers against optical feedback," Opt. Express **21**, 13748–13757 (2013).
[10] S. Zaminga, L. Columbo, C. Silvestri, M. Gioannini, and F. Grillot, "Impact of spatial hole burning and linewidth enhancement factor on distributed-feedback quantum cascade lasers: A comprehensive design analysis," IEEE Photonics J. **16**, 1–9 (2024).
[11] J. Ohtsubo, *Semiconductor Lasers: Stability, Instability and Chaos*, *Springer Series in Optical Sciences* (Springer International Publishing, 2017).
[12] C. Silvestri, L. L. Columbo, M. Brambilla, and M. Gioannini, "Coherent multi-mode dynamics in a quantum cascade laser: Amplitude- and frequency-modulated optical frequency combs," Opt. Express **28**, 23846–23861 (2020).
[13] C. Silvestri *et al.*, "Theory and modelization of quantum cascade laser dynamics: Comb formation, field structures and feedback-based imaging," Ph.D. thesis, Politecnico di Torino, Torino, 2022.
[14] B. Tromborg, H. Olesen, X. Pan, and S. Saito, "Transmission line description of optical feedback and injection locking for Fabry-Perot and DFB lasers," IEEE J. Quantum Electron. **23**, 1875–1889 (1987).
[15] C. Silvestri, X. Qi, T. Taimre, and A. D. Rakić, "Frequency combs induced by optical feedback and harmonic order tunability in quantum cascade lasers," APL Photonics **8**, 116102 (2023).
[16] N. Mustafa, L. Pesquera, C. Y. L. Cheung, and K. A. Shore, "Terahertz bandwidth prediction for amplitude modulation response of unipolar intersubband semiconductor lasers," IEEE Photonics Technol. Lett. **11**, 527–529 (1999).
[17] C. Y. L. Cheung, P. S. Spencer, and K. A. Shore, "Modulation bandwidth optimisation for unipolar intersubband semiconductor lasers," IEE Proc.-Optoelectron. **144**, 44–47 (1997).
[18] F. Rana and R. J. Ram, "Current noise and photon noise in quantum cascade lasers," Phys. Rev. B **65**, 125313 (2002).
[19] R. Paiella, R. Martini, F. Capasso, C. Gmachl, H. Y. Hwang, D. L. Sivco, J. N. Baillargeon, A. Y. Cho, E. A. Whittaker, and H. C. Liu, "High-frequency modulation without the relaxation oscillation resonance in quantum cascade lasers," Appl. Phys. Lett. **79**, 2526–2528 (2001).
[20] S. Barbieri, W. Maineult, S. S. Dhillon, C. Sirtori, J. Alton, N. Breuil, H. E. Beere, and D. A. Ritchie, "13 GHz direct modulation of terahertz quantum cascade lasers," Appl. Phys. Lett. **91**, 143510 (2007).
[21] W. Maineult, L. Ding, P. Gellie, P. Filloux, C. Sirtori, S. Barbieri, T. Akalin, J.-F. Lampin, I. Sagnes, H. E. Beere, and D. A. Ritchie, "Microwave modulation of terahertz quantum cascade lasers: A transmission-line approach," Appl. Phys. Lett. **96**, 021108 (2010).
[22] Y. Petitjean, F. Destic, S. Barbieri, C. Sirtori, and J.-C. Mollier, "Direct modulation and bandwidth measurement of terahertz quantum cascade laser," SPIE **7763**, 776306 (2010).
[23] C. Silvestri, X. Qi, T. Taimre, K. Bertling, and A. D. Rakić, "Frequency combs in quantum cascade lasers: An overview of modeling and experiments," APL Photonics **8**, 020902 (2023).
[24] M. Piccardo and F. Capasso, "Laser frequency combs with fast gain recovery: Physics and applications," Laser Photonics Rev. **16**, 2100403 (2022).
[25] R. Paiella, *Intersubband Transitions in Quantum Structures*, *McGraw-Hill Nanoscience and Technology Series* (McGraw Hill LLC, 2010).
[26] L. Jumpertz, F. Michel, R. Pawlus, W. Elsässer, K. Schires, M. Carras, and F. Grillot, "Measurements of the linewidth enhancement factor of mid-infrared quantum cascade lasers by different optical feedback techniques," AIP Adv. **6**, 015212 (2016).
[27] O. Spitz, A. Herdt, J. Duan, M. Carras, W. Elsässer, and F. Grillot, "Extensive study of the linewidth enhancement factor of a distributed feedback quantum cascade laser at ultra-low temperature," SPIE **10926**, 1092619 (2019).
[28] I. Vurgaftman and J. R. Meyer, "Analysis of limitations to wallplug efficiency and output power for quantum cascade lasers," J. Appl. Phys. **99**, 123108 (2006).

[29]B. G. Lee, M. A. Belkin, C. Pflugl, L. Diehl, H. A. Zhang, R. M. Audet, J. MacArthur, D. P. Bour, S. W. Corzine, G. E. Hofler, and F. Capasso, "DFB quantum cascade laser arrays," IEEE J. Quantum Electron. **45**, 554–565 (2009).
[30]M. K. Haldar, "A simplified analysis of direct intensity modulation of quantum cascade lasers," IEEE J. Quantum Electron. **41**, 1349–1355 (2005).
[31]P. Bardella, L. L. Columbo, and M. Gioannini, "Self-generation of optical frequency comb in single section quantum dot Fabry-Perot lasers: A theoretical study," Opt. Express **25**, 26234–26252 (2017).
[32]P. Glas, R. Müller, and A. Klehr, "Bistability, self-sustained oscillations, and irregular operation of a GaAs laser coupled to an external resonator," Opt. Commun. **47**, 297–301 (1983).
[33]D. Lenstra, B. Verbeek, and A. Den Boef, "Coherence collapse in single-mode semiconductor lasers due to optical feedback," IEEE J. Quantum Electron. **21**, 674–679 (1985).
[34]J. Sacher, W. Elsässer, and E. O. Göbel, "Intermittency in the coherence collapse of a semiconductor laser with external feedback," Phys. Rev. Lett. **63**, 2224 (1989).
[35]J. Mork, B. Tromborg, and P. L. Christiansen, "Bistability and low-frequency fluctuations in semiconductor lasers with optical feedback: A theoretical analysis," IEEE J. Quantum Electron. **24**, 123–133 (1988).
[36]J. Sacher, W. Elsasser, and E. O. Gobel, "Nonlinear dynamics of semiconductor laser emission under variable feedback conditions," IEEE J. Quantum Electron. **27**, 373–379 (1991).
[37]J. Mork, B. Tromborg, and J. Mark, "Chaos in semiconductor lasers with optical feedback: Theory and experiment," IEEE J. Quantum Electron. **28**, 93–108 (1992).
[38]I. Fischer, O. Hess, W. Elsäer, and E. Göbel, "High-dimensional chaotic dynamics of an external cavity semiconductor laser," Phys. Rev. Lett. **73**, 2188 (1994).
[39]M. Brandstetter and B. Lendl, "Tunable mid-infrared lasers in physical chemosensors towards the detection of physiologically relevant parameters in biofluids," Sens. Actuators, B **170**, 189–195 (2012).
[40]V. S. Serebryakov, É. V. Boĭko, A. G. Kalintsev, A. F. Kornev, A. S. Narivonchik, and A. L. Pavlova, "Mid-IR laser for high-precision surgery," J. Opt. Technol. **82**, 781–788 (2015).
[41]H. D. Tholl, "Review and prospects of optical countermeasure technologies," SPIE **10797**, 1079702 (2018).
[42]L. Jumpertz, K. Schires, M. Carras, M. Sciamanna, and F. Grillot, "Chaotic light at mid-infrared wavelength," Light: Sci. Appl. **5**, e16088 (2016).
[43]O. Spitz and F. Grillot, "A review of recent results of mid-infrared quantum cascade photonic devices operating under external optical control," J. Phys.: Photonics **4**, 022001 (2022).
[44]R. Lang and K. Kobayashi, "External optical feedback effects on semiconductor injection laser properties," IEEE J. Quantum Electron. **16**, 347–355 (1980).
[45]X. Qi, K. Bertling, T. Taimre, G. Agnew, Y. L. Lim, T. Gillespie, A. Robinson, M. Brünig, A. Demić, P. Dean, L. H. Li, E. H. Linfield, A. G. Davies, D. Indjin, and A. D. Rakić, "Observation of optical feedback dynamics in single-mode terahertz quantum cascade lasers: Transient instabilities," Phys. Rev. A **103**, 033504 (2021).
[46]P. Grassberger and I. Procaccia, "Characterization of strange attractors," Phys. Rev. Lett. **50**, 346 (1983).
[47]E. N. Lorenz, "Deterministic nonperiodic flow," J. Atmos. Sci. **20**, 130–141 (1963).
[48]O. Spitz, J. Wu, M. Carras, C.-W. Wong, and F. Grillot, "Low-frequency fluctuations of a mid-infrared quantum cascade laser operating at cryogenic temperatures," Laser Phys. Lett. **15**, 116201 (2018).
[49]L. L. Columbo and M. Brambilla, "Multimode regimes in quantum cascade lasers with optical feedback," Opt. Express **22**, 10105–10118 (2014).